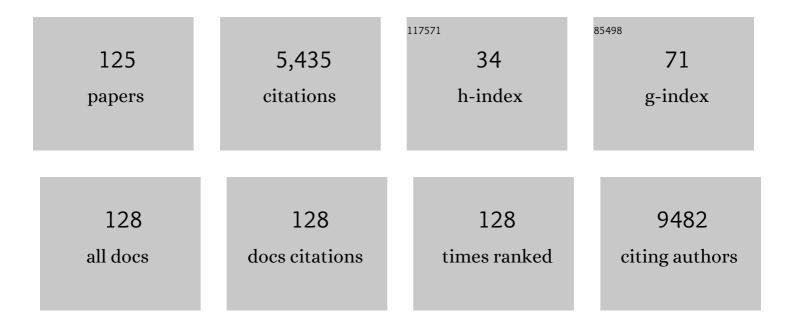
## Erdmann Spiecker

List of Publications by Year in descending order

Source: https://exaly.com/author-pdf/3699612/publications.pdf Version: 2024-02-01



#	Article	IF	CITATIONS
1	Scavenging of bacteria or bacterial products by magnetic particles functionalized with a broad-spectrum pathogen recognition receptor motif offers diagnostic and therapeutic applications. Acta Biomaterialia, 2022, 141, 418-428.	4.1	11
2	Overcoming Temperatureâ€Induced Degradation of Silver Nanowire Electrodes by an Ag@SnO <sub>x</sub> Coreâ€Shell Approach. Advanced Electronic Materials, 2022, 8, .	2.6	7
3	Quantification of the temperature-dependent evolution of defect structures in a CoNi-base superalloy. Acta Materialia, 2022, 227, 117702.	3.8	14
4	Noncovalent Liquid Phase Functionalization of 2H-WS <sub>2</sub> with PDI: An Energy Conversion Platform with Long-Lived Charge Separation. Journal of the American Chemical Society, 2022, 144, 5834-5840.	6.6	8
5	Exploring the Preparation Dependence of Crystalline 2D-Extended Ultrathin C8-BTBT-C8 Films. ACS Applied Materials & Interfaces, 2022, 14, 16830-16838.	4.0	6
6	Sub-Kelvin thermometry for evaluating the local temperature stability within in situ TEM gas cells. Ultramicroscopy, 2022, 235, 113494.	0.8	6
7	Creep properties and deformation mechanisms of single-crystalline <i>γ</i> ′-strengthened superalloys in dependence of the Co/Ni ratio. Philosophical Magazine, 2022, 102, 718-744.	0.7	3
8	Atomically resolved TEM imaging of covalently functionalised graphene. Npj 2D Materials and Applications, 2022, 6, .	3.9	3
9	Seeing structural evolution of organic molecular nano-crystallites using 4D scanning confocal electron diffractionÂ(4D-SCED). Nature Communications, 2022, 13, .	5.8	6
10	Understanding and Controlling the Evolution of Nanomorphology and Crystallinity of Organic Bulkâ€Heterojunction Blends with Solvent Vapor Annealing. Solar Rrl, 2022, 6, .	3.1	8
11	The effect of γ matrix channel width on the compositional evolution in a multi-component nickel-based superalloy. Scripta Materialia, 2022, 219, 114853.	2.6	2
12	Radiolysisâ€Driven Evolution of Gold Nanostructures – Model Verification by Scale Bridging In Situ Liquidâ€Phase Transmission Electron Microscopy and Xâ€Ray Diffraction. Advanced Science, 2022, 9, .	5.6	15
13	Intrinsic nano-diffusion-couple for studying high temperature diffusion in multi-component superalloys. Scripta Materialia, 2021, 192, 120-124.	2.6	8
14	Microscopic Deformation Modes and Impact of Network Anisotropy on the Mechanical and Electrical Performance of Five-fold Twinned Silver Nanowire Electrodes. ACS Nano, 2021, 15, 362-376.	7.3	23
15	Reduced grey brookite for noble metal free photocatalytic H <sub>2</sub> evolution. Journal of Materials Chemistry A, 2021, 9, 1168-1179.	5.2	26
16	Correlative Laboratory Nano T and 360° Electron Tomography of Macropore Structures in Hierarchical Zeolites. Advanced Materials Interfaces, 2021, 8, 2001154.	1.9	11
17	Phase evolution of Cu <sub>2</sub> ZnSnS <sub>4</sub> (CZTS) nanoparticles from <i>in situ</i> formed binary sulphides under solvothermal conditions. CrystEngComm, 2021, 23, 7944-7954.	1.3	5
18	LPE growth of Tb <sub>3</sub> Al <sub>5</sub> O <sub>12</sub> :Ce single crystalline film converters for WLED application. CrystEngComm, 2021, 23, 3212-3219.	1.3	12

#	Article	IF	CITATIONS
19	Accessing local electron-beam induced temperature changes during <i>in situ</i> liquid-phase transmission electron microscopy. Nanoscale Advances, 2021, 3, 2466-2474.	2.2	30
20	Efficient charge-transfer from diketopyrrolopyrroles to single-walled carbon nanotubes. Nanoscale, 2021, 13, 11544-11551.	2.8	4
21	ZnS Ultrathin Interfacial Layers for Optimizing Carrier Management in Sb <sub>2</sub> S <sub>3</sub> -based Photovoltaics. ACS Applied Materials & Interfaces, 2021, 13, 11861-11868.	4.0	20
22	Comprehensive, multidimensional and correlative particle characterization of a saxolite and talcum compound to support the understanding of complex separation processes. Microscopy and Microanalysis, 2021, 27, 934-937.	0.2	2
23	Early stages of phase decomposition in NiAu alloy thin films studied by in situ TEM using ultrafast quenching methods. Microscopy and Microanalysis, 2021, 27, 2692-2694.	0.2	Ο
24	Diffraction contrast analysis of dislocations in 2D materials using true dark-field and 4D-STEM in SEM. Microscopy and Microanalysis, 2021, 27, 1816-1819.	0.2	0
25	Combining in situ heating with transmission diffraction and imaging in SEM for investigation of early stages of solid-state dewetting. Microscopy and Microanalysis, 2021, 27, 1052-1054.	0.2	Ο
26	Multi-modal characterization of collagen fibril orientation in human cortical bone by a combination of quantitative polarized Raman spectroscopy, nanoscale X-ray computed tomography and 360° electron tomography. Microscopy and Microanalysis, 2021, 27, 96-101.	0.2	0
27	Correlative Zernike phase contrast X-ray nanotomography to determine the distribution and orientation of graphite particles in a carbon fiber reinforced epoxy resin for improved thermal conductivity. Microscopy and Microanalysis, 2021, 27, 944-946.	0.2	Ο
28	Correlative relationship between nanomorphology, crystallinity, texture and device efficiency of organic BHJ solar cells studied by energy-filtered TEM. Microscopy and Microanalysis, 2021, 27, 390-392.	0.2	0
29	In situ chip-based heating studies of metal-induced layer exchange and Si crystallization using STEM, LEND and SE imaging in SEM. Microscopy and Microanalysis, 2021, 27, 2696-2698.	0.2	1
30	Scanning confocal electron diffraction (SCED): high angular resolution diffraction imaging with order-of-magnitude improved dose efficiency. Microscopy and Microanalysis, 2021, 27, 194-197.	0.2	0
31	Extending lab-based X-ray nanotomography of low Z and porous materials to larger sample volumes without compromising resolution. Microscopy and Microanalysis, 2021, 27, 1218-1221.	0.2	1
32	Beam-induced heating at low electron fluxes during liquid phase transmission electron microscopy. Microscopy and Microanalysis, 2021, 27, 1040-1042.	0.2	0
33	A scale-bridging study of the influence of TCP phases on the mechanical properties of an additive manufactured Ni-base superalloy combining microcompression testing, X-ray nanotomography and TEM. Microscopy and Microanalysis, 2021, 27, 938-942.	0.2	0
34	Unraveling Structural Details in Ga-Pd SCALMS Systems Using Correlative Nano-CT, 360° Electron Tomography and Analytical TEM. Catalysts, 2021, 11, 810.	1.6	7
35	Yielding behavior of a single-crystalline γ'-strengthened Co-Ti-Cr superalloy. Scripta Materialia, 2021, 200, 113928.	2.6	16
36	Grain boundary mediated plasticity: A blessing for the ductility of metallic thin films?. Acta Materialia, 2021, 215, 117079.	3.8	18

#	Article	IF	CITATIONS
37	Effect of size and shape on the elastic modulus of metal nanowires. MRS Advances, 2021, 6, 665-673.	0.5	11
38	Rapid fabrication and interface structure of highly faceted epitaxial Ni-Au solid solution nanoparticles on sapphire. Acta Materialia, 2021, 220, 117318.	3.8	10
39	Distinct endocytosis and immune activation of poly(lactic-co-glycolic) acidÂnanoparticles prepared by single- and double-emulsion evaporation. Nanomedicine, 2021, 16, 2075-2094.	1.7	4
40	Early stages of high-temperature oxidation of Ni- and Co-base model superalloys: A comparative study using rapid thermal annealing and advanced electron microscopy. Corrosion Science, 2021, 191, 109744.	3.0	22
41	Well-separated water-soluble carbon dots <i>via</i> gradient chromatography. Nanoscale, 2021, 13, 13116-13128.	2.8	19
42	Structural characterization of α,ï‰-DH6T monolayer films grown at the liquid–liquid interface. Soft Matter, 2021, 17, 9765-9771.	1.2	3
43	Pt–Fe <sub>3</sub> O <sub>4</sub> , Pd–Fe <sub>3</sub> O <sub>4</sub> , and Au–Fe <sub>3</sub> O <sub>4</sub> Nanoheterodimers and Their Efficacy as Radiosensitizers in Cancer Therapy. ACS Applied Bio Materials, 2021, 4, 7879-7892.	2.3	4
44	Hydrogenated anatase TiO <sub>2</sub> single crystals: defects formation and structural changes as microscopic origin of co-catalyst free photocatalytic H <sub>2</sub> evolution activity. Journal of Materials Chemistry A, 2021, 9, 24932-24942.	5.2	7
45	Modelling the Radiolysis of Silver Nitrate Solutions in presence of Bromide Ions in Liquid-Phase Transmission Electron Microscopy. Microscopy and Microanalysis, 2021, 27, 103-104.	0.2	1
46	Correlative Nanoâ€Computed Tomography and Focused Ionâ€Beam Sectioning: A Case Study on a Coâ€Base Superalloy Oxide Scale. Advanced Engineering Materials, 2020, 22, 1900823.	1.6	4
47	Facile one-pot synthesis of water-soluble fcc FePt3 alloy nanostructures. SN Applied Sciences, 2020, 2, 1.	1.5	2
48	Area‣elective Growth of HfS <sub>2</sub> Thin Films via Atomic Layer Deposition at Low Temperature. Advanced Materials Interfaces, 2020, 7, 2001493.	1.9	10
49	Unraveling Complexity: A Strategy for the Characterization of Anisotropic Core Multishell Nanoparticles. Particle and Particle Systems Characterization, 2020, 37, 2000145.	1.2	3
50	Epitaxial Metal Halide Perovskites by Inkjetâ€Printing on Various Substrates. Advanced Functional Materials, 2020, 30, 2004612.	7.8	21
51	Strain-activated light-induced halide segregation in mixed-halide perovskite solids. Nature Communications, 2020, 11, 6328.	5.8	86
52	Collecting up to 115% of Singlet-Fission Products by Single-Walled Carbon Nanotubes. ACS Nano, 2020, 14, 8875-8886.	7.3	7
53	Buried Microphase Separation by Dynamic Interplay of Crystallization and Microphase Separation in Semicrystalline PEO-Rich PS- <i>b</i> -PEO Block Copolymer Thin Films. Macromolecules, 2020, 53, 5604-5613.	2.2	6
54	Bipolar-shell resurfacing for blue LEDs based on strongly confined perovskite quantum dots. Nature Nanotechnology, 2020, 15, 668-674.	15.6	541

#	Article	IF	CITATIONS
55	Effect of the Counteranion on the Formation Pathway of Cu <sub>2</sub> ZnSnS <sub>4</sub> (CZTS) Nanoparticles under Solvothermal Conditions. Inorganic Chemistry, 2020, 59, 1973-1984.	1.9	14
56	Crystal-structure of active layers of small molecule organic photovoltaics before and after solvent vapor annealing. Zeitschrift Fur Kristallographie - Crystalline Materials, 2020, 235, 15-28.	0.4	6
57	Unraveling the Complex Nanomorphology of Ternary Organic Solar Cells with Multimodal Analytical Transmission Electron Microscopy. Solar Rrl, 2020, 4, 2000114.	3.1	7
58	Segregation-assisted climb of Frank partial dislocations: An alternative route to superintrinsic stacking faults in L12-hardened superalloys. Acta Materialia, 2020, 191, 270-279.	3.8	26
59	Mechanical cleaning of graphene using in situ electron microscopy. Nature Communications, 2020, 11, 1743.	5.8	36
60	Atomic Structure and Chemical Composition of Planar Fault Structures in Co-Base Superalloys. Minerals, Metals and Materials Series, 2020, , 920-928.	0.3	2
61	Interface Molecular Engineering for Laminated Monolithic Perovskite/Silicon Tandem Solar Cells with 80.4% Fill Factor. Advanced Functional Materials, 2019, 29, 1901476.	7.8	43
62	Preparation of Graphene-Supported Microwell Liquid Cells for <em>In Situ</em> Transmission Electron Microscopy. Journal of Visualized Experiments, 2019, , .	0.2	6
63	Nanoparticles: In Situ Liquid Cell TEM Studies on Etching and Growth Mechanisms of Gold Nanoparticles at a Solid–Liquid–Gas Interface (Adv. Mater. Interfaces 20/2019). Advanced Materials Interfaces, 2019, 6, 1970126.	1.9	1
64	In Situ Liquid Cell TEM Studies on Etching and Growth Mechanisms of Gold Nanoparticles at a Solid–Liquid–Gas Interface. Advanced Materials Interfaces, 2019, 6, 1901027.	1.9	23
65	In Vitro Endothelialization of Surface-Integrated Nanofiber Networks for Stretchable Blood Interfaces. ACS Applied Materials & Interfaces, 2019, 11, 5740-5751.	4.0	11
66	Fabrication and structural characterization of diamond-coated tungsten tips. Diamond and Related Materials, 2019, 97, 107446.	1.8	7
67	Lowâ€ŧemperature oxidationâ€induced crack healing in Ti 2 Al 0.5 Sn 0.5 C–Al 2 O 3 composites. International Journal of Applied Ceramic Technology, 2019, 16, 1744-1751.	1.1	2
68	Transforming layered MoS <sub>2</sub> into functional MoO <sub>2</sub> nanowires. Nanoscale, 2019, 11, 11687-11695.	2.8	12
69	Insights into fundamental deformation processes from advanced in situ transmission electron microscopy. MRS Bulletin, 2019, 44, 443-449.	1.7	16
70	Pushing PbS/Metalâ€Halideâ€Perovskite Core/Epitaxialâ€Ligandâ€5hell Nanocrystal Photodetectors beyond 3 µm Wavelength. Advanced Functional Materials, 2019, 29, 1807964.	7.8	35
71	Scanning Transmission Electron Microscopy and Diffraction in SEM: Novel Approaches for In Situ Studies. Microscopy and Microanalysis, 2019, 25, 25-26.	0.2	Ο
72	Determination of 3D electrostatic field at an electron nano-emitter. Applied Physics Letters, 2019, 114, 013101.	1.5	14

#	Article	IF	CITATIONS
73	Tension/Compression asymmetry of a creep deformed single crystal Co-base superalloy. Acta Materialia, 2019, 166, 597-610.	3.8	48
74	Assembling Mesoscaleâ€&tructured Organic Interfaces in Perovskite Photovoltaics. Advanced Materials, 2019, 31, e1806516.	11.1	16
75	Pressure induced local phase transformation in nanocrystalline tetragonal zirconia microparticles. Scripta Materialia, 2019, 163, 86-90.	2.6	4
76	Germanium Template Assisted Integration of Gallium Arsenide Nanocrystals on Silicon: A Versatile Platform for Modern Optoelectronic Materials. Advanced Optical Materials, 2018, 6, 1701329.	3.6	0
77	On the grain boundary strengthening effect of boron in γ/γ′ Cobalt-base superalloys. Acta Materialia, 2018, 145, 247-254.	3.8	73
78	Early stages of scale formation during oxidation of γ / γ ′ strengthened single crystal ternary Co-base superalloy at 900â€ <sup>-</sup> °C. Corrosion Science, 2018, 135, 78-86.	3.0	56
79	Impact of N Incorporation on VLS Growth of GaP(N) Nanowires Utilizing UDMH. Nanoscale Research Letters, 2018, 13, 417.	3.1	11
80	Understanding the Role of Surface Charge in Cellular Uptake and X-ray-Induced ROS Enhancing of Au–Fe <sub>3</sub> O <sub>4</sub> Nanoheterodimers. ACS Applied Bio Materials, 2018, 1, 2002-2011.	2.3	14
81	Inducing a Nanotwinned Grain Structure within the TiO <sub>2</sub> Nanotubes Provides Enhanced Electron Transport and DSSC Efficiencies >10%. Advanced Energy Materials, 2018, 8, 1800981.	10.2	42
82	Unravelling the Mechanisms of Gold–Silver Core–Shell Nanostructure Formation by in Situ TEM Using an Advanced Liquid Cell Design. Nano Letters, 2018, 18, 7222-7229.	4.5	57
83	Thermophysical and Mechanical Properties of Advanced Single Crystalline Co-base Superalloys. Metallurgical and Materials Transactions A: Physical Metallurgy and Materials Science, 2018, 49, 4099-4109.	1.1	58
84	In situ manipulation and switching of dislocations in bilayer graphene. Science Advances, 2018, 4, eaat4712.	4.7	33
85	Elemental segregation to antiphase boundaries in a crept CoNi-based single crystal superalloy. Scripta Materialia, 2018, 157, 62-66.	2.6	48
86	On the diffusive phase transformation mechanism assisted by extended dislocations during creep of a single crystal CoNi-based superalloy. Acta Materialia, 2018, 155, 362-371.	3.8	89
87	Butterfly gyroid nanostructures as a time-frozen glimpse of intracellular membrane development. Science Advances, 2017, 3, e1603119.	4.7	109
88	Direct observation of dislocation formation and plastic anisotropy in Nb2AlC MAX phase using in situ nanomechanics in transmission electron microscopy. Scripta Materialia, 2017, 137, 104-108.	2.6	14
89	Publisher's note. Ultramicroscopy, 2017, 177, 1-13.	0.8	1
90	Correlative micro-diffraction and differential phase contrast study of mean inner potential and subtle beam-specimen interaction. Ultramicroscopy, 2017, 176, 233-245.	0.8	11

#	Article	IF	CITATIONS
91	Suppression of Hysteresis Effects in Organohalide Perovskite Solar Cells. Advanced Materials Interfaces, 2017, 4, 1700007.	1.9	57
92	Local temperature measurement in TEM by parallel beam electron diffraction. Ultramicroscopy, 2017, 176, 161-169.	0.8	67
93	Nanoscale distribution of Bi atoms in InP1â^'xBix. Scientific Reports, 2017, 7, 12278.	1.6	7
94	Deformation behavior of nanocrystalline titania particles accessed by complementary inÂsitu electron microscopy techniques. Journal of the American Ceramic Society, 2017, 100, 5709-5722.	1.9	15
95	Memory Effect of Selfâ€Assembled PSâ€ <i>b</i> â€PEO Block Copolymer Films with Selectively Embedded Functionalized TiO <sub>2</sub> Nanoparticles. Advanced Materials Interfaces, 2017, 4, 1700230.	1.9	13
96	A generic interface to reduce the efficiency-stability-cost gap of perovskite solar cells. Science, 2017, 358, 1192-1197.	6.0	554
97	Low temperature solid-state wetting and formation of nanowelds in silver nanowires. Nanotechnology, 2017, 28, 385701.	1.3	7
98	Overcoming the Interface Losses in Planar Heterojunction Perovskiteâ€Based Solar Cells. Advanced Materials, 2016, 28, 5112-5120.	11.1	188
99	Planar defect formation in the γ′ phase during high temperature creep in single crystal CoNi-base superalloys. Acta Materialia, 2016, 113, 335-349.	3.8	108
100	High efficiency and stability small molecule solar cells developed by bulk microstructure fine-tuning. Nano Energy, 2016, 28, 241-249.	8.2	57
101	A flexible method for the preparation of thin film samples for in situ TEM characterization combining shadow-FIB milling and electron-beam-assisted etching. Ultramicroscopy, 2016, 171, 82-88.	0.8	13
102	Organic and perovskite solar modules innovated by adhesive top electrode and depth-resolved laser patterning. Energy and Environmental Science, 2016, 9, 2302-2313.	15.6	64
103	Texture evolution and microstructural changes during solid-state dewetting: A correlative study by complementary in situ TEM techniques. Acta Materialia, 2016, 115, 230-241.	3.8	23
104	Crack healing induced electrical and mechanical properties recovery in a Ti 2 SnC ceramic. Journal of the European Ceramic Society, 2016, 36, 25-32.	2.8	42
105	Photophysics of Molecularâ€Weightâ€Induced Losses in Indacenodithienothiopheneâ€Based Solar Cells. Advanced Functional Materials, 2015, 25, 4898-4907.	7.8	61
106	A New Crystal Phase Molybdate Yb <sub>2</sub> Mo <sub>4</sub> O <sub>15</sub> : The Synthesis and Upconversion Properties. Particle and Particle Systems Characterization, 2015, 32, 340-346.	1.2	11
107	Uniform Surface Modification of 3D Bioglass®-Based Scaffolds with Mesoporous Silica Particles (MCM-41) for Enhancing Drug Delivery Capability. Frontiers in Bioengineering and Biotechnology, 2015, 3, 177.	2.0	29
108	A comprehensive study on the mechanism behind formation and depletion of Cu <sub>2</sub> ZnSnS <sub>4</sub> (CZTS) phases. CrystEngComm, 2015, 17, 6972-6984.	1.3	37

#	Article	IF	CITATIONS
109	The process of solid-state dewetting of Au thin films studied by in situ scanning transmission electron microscopy. Acta Materialia, 2015, 90, 118-132.	3.8	71
110	On the identification of superdislocations in the γ′-phase of single-crystal Ni-base superalloys – An application of the LACBED method to complex microstructures. Acta Materialia, 2015, 87, 34-44.	3.8	17
111	Advanced Scale Bridging Microstructure Analysis of Single Crystal Niâ€Base Superalloys. Advanced Engineering Materials, 2015, 17, 216-230.	1.6	117
112	The effects of post-processing on the surface and the optical properties of copper indium sulfide quantum dots. Journal of Colloid and Interface Science, 2015, 445, 337-347.	5.0	22
113	Encapsulation of silver nanowire networks by atomic layer deposition for indium-free transparent electrodes. Nano Energy, 2015, 16, 196-206.	8.2	68
114	Coexistence of both gyroid chiralities in individual butterfly wing scales of <i>Callophrys rubi</i> . Proceedings of the National Academy of Sciences of the United States of America, 2015, 112, 12911-12916.	3.3	58
115	Influence of anisotropic elasticity on the mechanical properties of fivefold twinned nanowires. Journal of the Mechanics and Physics of Solids, 2015, 84, 358-379.	2.3	37
116	"Black―TiO <sub>2</sub> Nanotubes Formed by High-Energy Proton Implantation Show Noble-Metal- <i>co</i> -Catalyst Free Photocatalytic H <sub>2</sub> -Evolution. Nano Letters, 2015, 15, 6815-6820.	4.5	174
117	Combining Atomistic Simulation and X-ray Diffraction for the Characterization of Nanostructures: A Case Study on Fivefold Twinned Nanowires. ACS Nano, 2014, 8, 1629-1638.	7.3	34
118	Epitaxial Growth of PbSe Quantum Dots on MoS <sub>2</sub> Nanosheets and their Nearâ€Infrared Photoresponse. Advanced Functional Materials, 2014, 24, 5798-5806.	7.8	134
119	A significant cathodic shift in the onset potential of photoelectrochemical water splitting for hematite nanostructures grown from Fe–Si alloys. Materials Horizons, 2014, 1, 344-347.	6.4	15
120	Black TiO <sub>2</sub> Nanotubes: Cocatalyst-Free Open-Circuit Hydrogen Generation. Nano Letters, 2014, 14, 3309-3313.	4.5	417
121	Broadband NIR photoluminescence from Ni <sup>2+</sup> -doped nanocrystalline Ba–Al titanate glass ceramics. Journal of Materials Chemistry, 2012, 22, 2582-2588.	6.7	47
122	Bioactive glass (type 45S5) nanoparticles: in vitro reactivity on nanoscale and biocompatibility. Journal of Nanoparticle Research, 2012, 14, 1.	0.8	114
123	Covalent bulk functionalization of graphene. Nature Chemistry, 2011, 3, 279-286.	6.6	596
124	Epitaxial upward transport of Al at the beginning of the Alâ€induced layer exchange process. Physica Status Solidi - Rapid Research Letters, 2011, 5, 172-174.	1.2	2
125	Nonâ€Covalent Chemistry of Graphene: Electronic Communication with Dendronized Perylene Bisimides. Advanced Materials, 2010, 22, 5483-5487.	11.1	120